Available online at www.sciencedirect.com
SCIENCE DIRECT®
Journal of Nuclear Materials 353 (2006) 147–157
journal of nuclear materials
www.elsevier.com/locate/jnucmat

Incorporation of cerium and neodymium in uranyl phases

Cheol-Woon Kim [a,*], David J. Wronkiewicz [b], Robert J. Finch [c], Edgar C. Buck [d]

[a] Department of Mining and Nuclear Engineering, University of Missouri-Rolla, Rolla, MO 65409, USA
[b] Department of Geological Sciences and Engineering, University of Missouri-Rolla, Rolla, MO 65409, USA
[c] Argonne National Laboratory, 9700 S. Cass Avenue, Argonne, IL 60439, USA
[d] Pacific Northwest National Laboratory, P.O. Box 999, Richland, WA 99352, USA

Received 29 July 2005; accepted 3 February 2006

Abstract

The potential for incorporating rare earth elements (REE) into/onto crystalline compounds has been evaluated by precipitating uranyl phases from aqueous solutions containing either cerium or neodymium. These REEs serve both as monitors for evaluating the potential repository behavior of REE radionuclides, and as surrogate elements for actinides (e.g., Ce^{4+} and Nd^{3+} for Pu^{4+} and Am^{3+}, respectively). The present experiments examined the behavior of REE in the presence of ianthinite ($[U_2^{4+}(UO_2)_4O_6(OH)_4(H_2O)_4](H_2O)_5$), becquerelite ($Ca(UO_2)_6O_4(OH)_6(H_2O)_8$), and other uranyl hydroxide compounds commonly noted as alteration products during the corrosion of UO_2, spent nuclear fuel, and naturally occurring uraninite. The results of these experiments demonstrate that significant quantities of both cerium ($K_d = 1020$) and neodymium ($K_d = 840$) are incorporated within the uranium alteration phases and suggest that ionic substitution and/or adsorption to the uranyl phases can play a key role in the limiting the mobility of REE (and by analogy, actinide elements) in a nuclear waste repository.

PACS: 28.41.Kw

1. Introduction

Spent nuclear fuel typically contains $\geqslant 95\%$ UO_2, up to 1% Pu, with the remainder including transuranic elements (e.g., Np, Am, Cm) and fission products (e.g., Sr, Cs, Tc, I, Mo, Se) [1]. The UO_2 matrix of spent nuclear fuel is unstable in the presence of a moist oxidizing atmosphere and may rapidly dissolve under such conditions which are expected to exist at the proposed nuclear waste repository at Yucca Mountain, Nevada [2,3]. Actinides and other radionuclides contained in the spent fuel may be released under such a scenario and would be a cause for concern if they were released into the environment. Laboratory studies examining the alteration of UO_2, spent nuclear fuel, and studies of natural uranium occurrences in arid to semi-arid settings have shown that most of the uranium released during UO_2 dissolution will reprecipitate as uranyl alteration phases due to the relatively low solubility of uranium and limited amount of

* Corresponding author. Tel.: +1 573 341 4359; fax: +1 573 341 6309.
E-mail address: cheol@umr.edu (C.-W. Kim).

0022-3115/$ - see front matter © 2006 Elsevier B.V. All rights reserved.
doi:10.1016/j.jnucmat.2006.02.087

water available for transport [2–5]. Actinide elements such as Np, and fission product isotopes of Cs, Sr, and Mo are also incorporated into these alteration phases [3,6–8]. Such a process may thus retard the migration of radionuclides in a repository setting.

The purpose of this study is to characterize the potential for the incorporation of Pu^{4+} and Am^{3+} into uranium phases by synthesizing uranyl compounds in the presence of Ce^{4+} or Nd^{3+}. The crystal chemistry of Ce^{4+} and Nd^{3+} are expected to simulate that of Pu^{4+} and Am^{3+} because of the similarity of valence charges and ionic radii between the various species (e.g., Ce^{4+} 0.094 nm vs. Pu^{4+} 0.093 nm; Nd^{3+} 0.104 nm vs. Am^{3+} 0.107 nm [9]). Thus, Ce^{4+} and Nd^{3+} are being used as proxies in these tests for Pu^{4+} and Am^{3+}, respectively. Results from this study may provide useful data for estimating realistic release rates for radionuclides from a near-field repository environment. The uranyl phases examined in this study include ianthinite ($[U_2^{4+}(UO_2)_4O_6(OH)_4(H_2O)_4](H_2O)_5$), becquerelite ($Ca(UO_2)_6O_4(OH)_6(H_2O)_8$), and other uranyl hydroxide compounds. Ianthinite is a mixed valence uranium phase noted as an alteration product in natural uranium deposits and is of special interest with respect to actinide retention because it contains both U^{4+} and U^{6+} in its crystal structure [10–12]. This phase thus has the potential to directly incorporate tetravalent transuranic ions without the need for any charge compensating mechanism. Ianthinite is also expected to precipitate at the redox front between oxidized aqueous fluids and the reduced UO_2 spent fuel matrix, thus it is likely to be one of the first alteration phases that any released actinides from spent fuel may encounter. Becquerelite is a common alteration product of spent fuel, and it is among the earliest phases to form [2,3,13].

2. Experimental

2.1. Preparation of Ce and Nd solutions

Leachant solutions were prepared by dissolving cerium-IV oxide (CeO_2) or neodymium-III acetate hydrate ($(CH_3CO_2)_3Nd \cdot xH_2O$) into high-purity deionized water (resistance $\geqslant$ 18.0 MΩ/cm). The cerium oxide and neodymium acetate were both certified to >99.9% purity. Both solutions were acidified to a pH of 4 with HNO_3 (Optima grade) to increase the solubility of the rare earth elements (REE) in solution. The leachants were placed in a 90 °C oven for 5 days, with the samples being occasionally agitated to promote dissolution. The solutions were then passed through a 0.45 μm syringe filter prior to use. Solution analyses indicate a composition of 2.1 wppm cerium for the leachant used in the 7- and 35-day tests, 4.6 wppm cerium for the 190-day tests, and 277–399 wppm neodymium for the 7- and 35-day tests.

2.2. Precipitation tests

Ianthinite was produced by dissolving 0.32 g of uranium oxyacetate ($UO_2(CH_3COO)_2 \cdot 2H_2O$) and 0.08 g of copper acetate monohydrate ($Cu(C_2H_3O_2)_2 \cdot H_2O$) for the partial reduction of U^{6+} into a 15 ml solution containing either 2.1 wppm cerium or 399 wppm neodymium. Additional tests with Nd concentrations (9.8 wppm) approximating those of Ce (2.1 wppm) were conducted at a later stage of the study to assess differences in atomic substitution between the two lanthanide elements from solutions with similar ionic strengths and the same lanthanide element at different atomic strengths. The solution was transferred into Teflon-lined Parr reaction bombs which were tightened with an external compression fitting. The bombs were heated at 150 ± 2 °C in an automated temperature-controlled ovens for 7 days. Copper acetate, at 140 °C, decomposes to Cu^{2+} and Cu^{+}, the latter which plays a role as a reducing agent for uranium [14]. The reducing mechanisms of U^{6+} are as follows:

$$Cu^{+} \rightarrow Cu^{2+} + e^{-} \quad (1)$$

$$UO_2^{2+} + 4H^{+} + 2e^{-} \rightarrow U^{4+} + 2H_2O \quad (2)$$

The precipitation of ianthinite is represented by the reaction:

$$2U^{4+} + 4UO_2^{2+} + 19H_2O \rightarrow [U_2^{4+}(UO_2)_4O_6(OH)_4(H_2O)_4](H_2O)_5 + 16H^{+} \quad (3)$$

After 7 days, the reaction bombs were removed from the oven and cooled to room temperature. The leachate solution was prepared for inductively coupled plasma–mass spectrometry (ICP–MS) analysis by passing through a preheated 0.45 μm syringe filter and then acidifying with optima grade HNO_3. The precipitates consisted of fine-grained purple crystals of ianthinite, small crystals of cuprite (Cu_2O) and tenorite (CuO). The crystals that formed were rinsed three times with deionized water and then air-dried.

Becquerelite was obtained by dissolving 0.42 g of uranium oxyacetate and 0.35 g of calcium acetate ($(CH_3COO)_2Ca \cdot H_2O$) in a 20 ml solution containing either 2.1 wppm cerium or 277 wppm neodymium. The precipitation of becquerelite is represented by the reaction:

$$6UO_2^{2+} + Ca^{2+} + 18H_2O \rightarrow Ca(UO_2)_6O_4(OH)_6(H_2O)_8 + 14H^+ \quad (4)$$

Test solutions were maintained in Teflon vessels that were heated to 90 ± 2 °C for 7 days. The lids of the vessels were quickly opened and re-closed for the first few days to vent any volatile acetic acid, providing better conditions for the precipitation of solid phase and possibly reducing the potential for the formation of lanthanide complexes with acetate. After cooling to room temperature, the precipitates consisted of fine platy yellow crystals of becquerelite. The solid products that formed were rinsed three times with deionized water and then air-dried. The leachate solution was prepared for ICP–MS analysis in the same manner as with the ianthinite tests.

Precipitation tests for uranyl hydroxide phases were conducted by adding 0.42 g of uranium oxyacetate into a Teflon vessel and then adding 20 ml of leachant solution containing either 2.1 wppm Ce, 4.6 wppm Ce, or 286 wppm Nd. The Teflon vessels were then sealed and placed in a mechanical convection oven maintained at a temperature of 90 ± 2 °C. The lids on the vessels were periodically open and closed for the first few days of testing to allow for venting of acetic acid. Experiments were conducted for intervals of 7, 35, and 190 days. After the prescribed test interval, the vessels were removed from the oven and the leachate solution was prepared for ICP–MS analysis. The solid uranium reaction products that formed were rinsed three times with deionized water and then allowed to air dry.

2.3. Solution and solid analysis

An analysis of the leachate solutions and solid phase reaction products (after dissolution in a nitric acid solution) was performed using a Perkin–Elmer ELAN-5000 ICP–MS. Duplicate analyses demonstrate an analytical precision of 0.5% and 6.7% for the cerium and neodymium analyses, respectively. Accuracy values for the cerium and neodymium analysis were within ±5% or better.

A small portion of the solid phase reaction products were transferred onto aluminum mounts, coated with carbon, and examined in a JEOL T330A scanning electron microscope (SEM) equipped with an energy dispersive X-ray spectrometer (EDS). Additional portions of the samples were secured onto low-background silicon plates by drying in a few drops of ethanol. These mounts were analyzed by X-ray diffraction (XRD) using a Rigaku Miniflex X-ray diffractometer. Reaction products from selected samples were also crushed into electron-transparent thin-section particles. These particles were transferred onto holey carbon-coated copper grids and examined using a JEOL 2000 FX II analytical transmission electron microscope (AEM) housed at Argonne National Laboratory. The AEM is equipped with a Gatan 666 parallel electron energy-loss spectrometer (EELS), which has an energy resolution of about 1.6–1.8 eV. Electron diffraction patterns were taken with a charge-coupled camera device (CCD) that permits low intensity viewing for electron-beam sensitive materials like the uranium phases formed in this study. Electron diffraction patterns obtained from the samples were compared to the Desktop Microscopist computer simulations utilizing the inorganic crystal structure database produced jointly by Fachinformationszentrum FIZ Karlsruhe and Gmelin-Institut für Anorganische Chemie.

3. Results and discussion

3.1. Solid phase analysis

3.1.1. Ianthinite

SEM examination of the solid phase reaction products from 7-day tests demonstrated the presence of radiating masses of crystalline ianthinite (Fig. 1(a)). Fig. 1(b) shows an AEM image of the ianthinite particles. The computer simulations of the ianthinite structure partially matched those with the experimentally obtained CCD electron diffraction pattern from the uranium phase shown in the inset of Fig. 1(b), but extra diffraction patterns appeared, suggesting the presence of an additional phase. There are several factors that may contribute to the pattern-matching difficulties. These particles were noted to slowly and progressively change from the purple color of ianthinite to a yellowish color more characteristic of dehydrated schoepite following their removal from the test solutions. The sample that was examined by AEM may therefore have

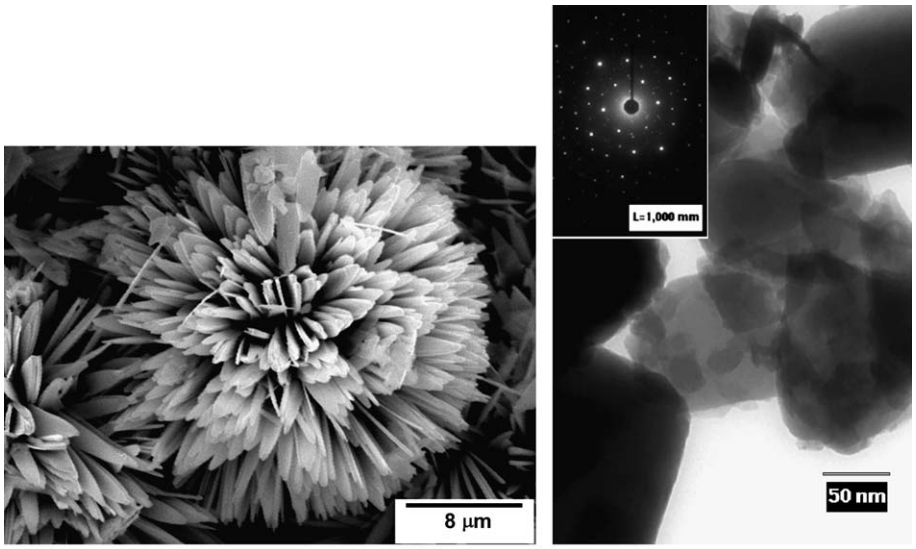

Fig. 1. (a) SEM micrograph of ianthinite crystals from 7-day tests, (b) AEM bright field image of ianthinite particles (inset: selected area electron diffraction pattern from ianthinite).

been partially oxidized to a schoepite type phase between the time the test was terminated and the sample was analyzed. In addition to the potential for oxidation, dehydration in the vacuum chamber during analysis could lead to structural rearrangement in the crystals [15]. Finally, there is limited amount of information on atomic parameters of ianthinite for the computer simulations. Ianthinite was also readily identified from powder XRD patterns (JCPDS-ICDD card #12-0272) because of an intense peak corresponding to 0.76 nm (*d*-spacing) and a few intense peaks at 0.38–0.32 nm and some of the patterns matched those of tenorite (CuO, JCPDS-ICDD card #05-0661) and cuprite (Cu_2O, JCPDS-ICDD card #05-0667). Peaks matching those of dehydrated schoepite were not observed.

3.1.2. Becquerelite

Examination of the solid phase reaction products with SEM indicates the presence of platy crystals of becquerelite (Fig. 2(a)). The AEM image of the uranyl phase also shows the characteristic platy morphology of becquerelite and the computer simulations of the becquerelite structure agreed with the experimentally obtained CCD electron diffraction pattern from the uranyl phase shown in Fig. 2(b). Becquerelite was also readily identified from powder XRD patterns (JCPDS-ICDD card #13-0405, 08-0299) because of an intense peak corresponding to 0.75 nm.

3.1.3. Uranyl hydroxide compounds

The present experiments attempted to examine the aqueous behavior of REE in the presence of dehydrated schoepite ($((UO_2)O_{0.25-x}(OH)_{1.5+2x}$ ($0 < x < 0.25$)). This phase is commonly noted to form during the corrosion of UO_2, spent nuclear fuel, and naturally occurring uraninite [2–5,13,16]. AEM images of the crystals formed in the tests denote a boat-shaped morphology (Fig. 3(a)), with electron diffraction patterns that correlate with unit cell parameters for dehydrated schoepite (Fig. 3(b) [17]). However, XRD peaks obtained from the samples do not show the same correlation with the dehydrated schoepite phase. These patterns, rather, are consistent with the presence of a uranyl hydroxide ($UO_2(OH)_2$, JCPDS-ICDD #30-1403), although many of the XRD spectral peaks show a systematic small shift to lower *d*-spacings relative to the cataloged JCPDS-ICDD peaks. While the presence of dehydrated schoepite cannot be ruled out (based upon the electron diffraction pattern obtained from a single sample), this phase cannot be present in amounts significant enough to give rise to discernable XRD peaks.

3.2. Distribution of cerium and neodymium

3.2.1. Ianthinite

The Eh environment necessary to reduce some U^{6+} to U^{4+} may also be sufficiently reducing to

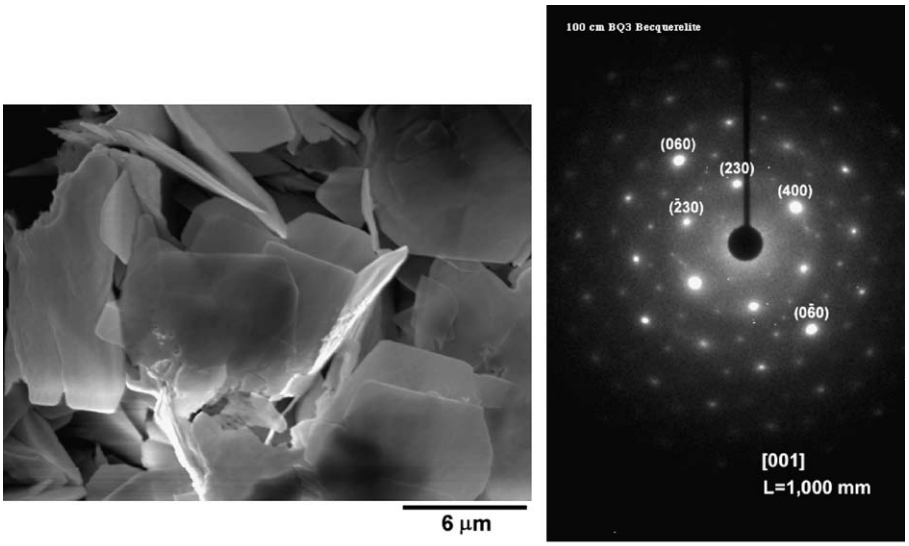

Fig. 2. (a) SEM micrograph of platy becquerelite crystals formed after 7 days of testing, (b) AEM selected area electron diffraction pattern from becquerelite particle.

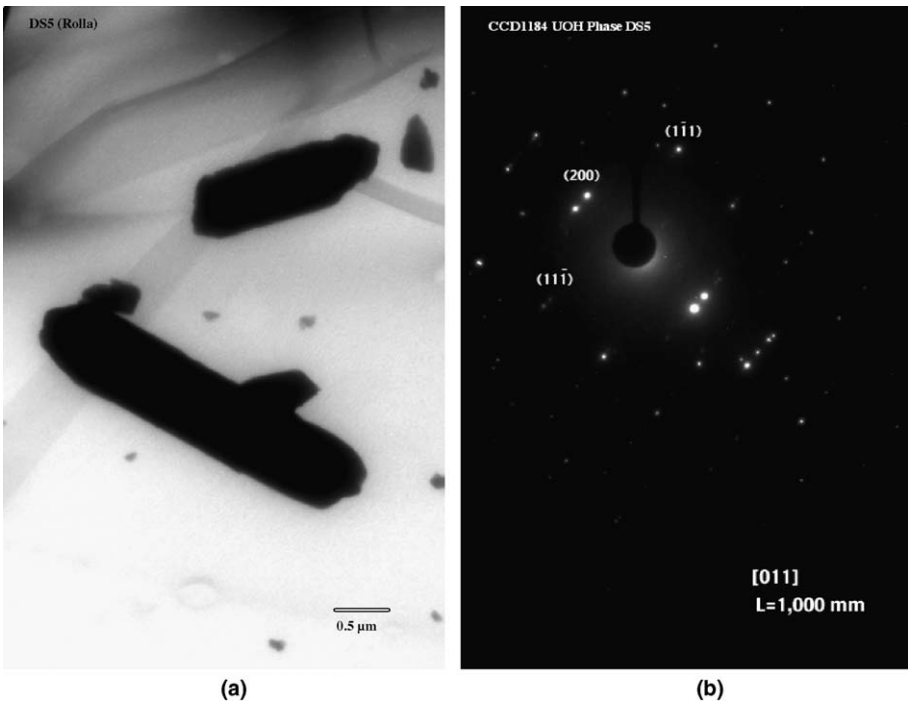

Fig. 3. (a) AEM bright field image of uranyl particle, (b) selected area electron diffraction pattern with match to dehydrated schoepite.

convert Ce^{4+} to Ce^{3+} in solution. Based on electrochemical reduction potentials [18], Ce^{4+} in solution might also convert to Ce^{3+} before the U^{6+} reduces to U^{4+}. Their reduction potentials (E°) in volts at standard conditions (25 °C and 1 atm) are as follows:

$$Ce^{4+} + e^- \rightarrow Ce^{3+}, \quad E^0 = 1.61, \tag{5}$$

$$UO_2^{2+} + 4H^+ + 2e^- \rightarrow U^{4+} + 2H_2O, \quad E^0 = 0.327. \tag{6}$$

The starting leachant compositions for Ce and Nd tests were 2.1 wppm and 399 wppm, respectively.

The ICP–MS results (Table 1) from dissolved solids indicate that about 306 wppm Ce was present in the ianthinite, while the neodymium content was much higher, being approximately 24 800 wppm. The distribution coefficient (K_d) was calculated using the equation:

$$K_d = \frac{C^x}{C^l}, \tag{7}$$

where C^x is the concentration of a minor element in a solid phase and C^l is the concentration of that element in leachate from which the solid phase formed. Concentration was used instead of activity for the ease of calculation, assuming that significant amounts of other cations and anions were not expect to be present in the test system except the uranyl and uranous ions. The potential effect of the presence of the additional phases including tenorite and cuprite on the distribution of Ce and Nd in the ianthinite was neglected in this study.

The corresponding K_d values for Ce and Nd incorporation in this test were 1020 and 115, respectively. The K_d value of cerium appeared higher than that of neodymium, implying that incorporation of cerium may be favored over the incorporation of neodymium in ianthinite. However, differences in ionic strength of the respective lanthanide solutions may also have an effect on these K_d values. Additional tests with Nd leachant concentrations (9.8 wppm) approximating those of Ce (2.1 wppm) showed that the K_d for Nd retention in ianthinite was 840, indicating that K_d for Nd rose with the falling Nd concentration in starting leachant. The K_d of Nd^{3+} was also similar to that of cerium bearing solutions with similar ionic strengths. This suggests that the ionic potential of neodymium in the tests at 9.8 wppm is similar to that of cerium at 2.1 wppm and implies that there is little preference between the incorporation of cerium and neodymium in ianthinite. Such a trend suggests that Ce^{4+} might have been reduced to Ce^{3+} in test solutions, thus explaining its similar behavior to Nd^{3+}.

Table 1
K_d values for Ce and Nd in ianthinite

	Leachant (wppm)	Leachate (wppm)	Ianthinite (wppm)[a]	K_d
Ce^{4+} and/or Ce^{3+}	2.1	0.3	306	1020
Nd^{3+}	399	216	24 800	115
Nd^{3+}	9.8	0.7	588	840

[a] Determined from ICP/MS analysis of the dissolved solids.

The K_d values of the lanthanides in ianthinite decreased with their increasing concentration in solution. If surface adsorption is involved as well as ionic substitution in these ianthinite tests, such a pattern may also be interpreted by the Freundlich or Langmuir adsorption isotherms [19], which indicate that the maximum K_d is found at the lowest concentration of a component in solution. Three data points from Table 1 are plotted on the Freundlich isotherm in Fig. 4 constructed by using the equation:

$$m_{ads} = K_d m_{soln}^n \tag{8}$$

where m_{ads} is the adsorbed element concentration in solid, m_{soln} is the element concentration in solution, and K_d and n are empirical constants (52 and 1/2 used in this study, respectively). In Fig. 4, the points fall along the Freundlich isotherm suggesting a possible surface adsorption effect for REE. At a high concentration (216 wppm in leachate), neodymium may have occupied many of available adsorption sites such as surface defects, and its further adsorption may be limited.

The potential for the incorporation of the REE into the crystalline structure of ianthinite was also evaluated in addition to the potential effects of surface adsorption. Solid phase examinations using AEM/EELS detected the presence of neodymium in the ianthinite crystals (Fig. 5), while the cerium content (initially determined from ICP/MS analysis of the dissolved solids) was below the detection limit of the AEM/EELS technique. The peak ratio of Nd/O (oxygen peak not shown in Fig. 5) was homogeneous (0.015–0.020) throughout the samples suggesting that Nd was uniformly distributed in the structure of ianthinite. The incorporation of

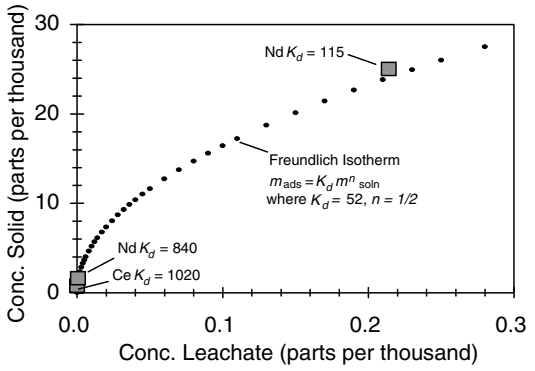

Fig. 4. Cerium and neodymium data plots on the Freundlich adsorption isotherm.

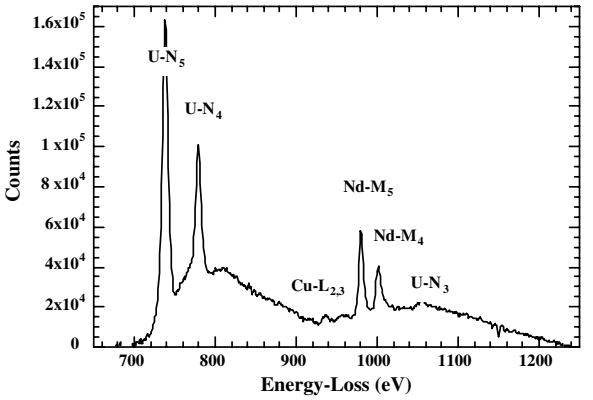

Fig. 5. Electron energy-loss spectrum of Nd-bearing ianthinite. $M_{4,5}$ edges of Nd are clearly visible. Lines for Cu are an artifact of the sample mounting medium.

Ce^{4+} into this structure, if present, is likely to occur by direct substitution for U^{4+} within the $U^{4+}\phi_6$ distorted octahedron polyhedral sheet [12] due to the similarity of valence charges and their bond lengths with anion ligands. According to the electrochemical reduction potentials and overlapping K_d results for cerium and neodymium, however, Ce^{4+} might have been converted to Ce^{3+}. If this reduction reaction occurred, the Ce^{3+} incorporation mechanism would be similar to that of Nd^{3+} discussed below.

The incorporation of Nd^{3+} into the ianthinite structure requires an appropriate charge compensating mechanism. One possible mechanism involves $OH^- \leftrightarrow O^{2-}$ [6], with the suggested charge-coupled substitution being $Nd^{3+} + OH^- \leftrightarrow U^{4+} + O^{2-}$. The balanced reaction for the substitution of Nd^{3+} into U^{4+} sites in ianthinite is proposed:

$$[U_2^{4+}(UO_2)_4O_6(OH)_4(H_2O)_4](H_2O)_5 + xNd^{3+} \Updownarrow [U_{2-x}^{4+}Nd_x(UO_2)_4O_{6-x}(OH)_{4+x}(H_2O)_4](H_2O)_5 + xU^{4+} - xH^+ \quad (9)$$

where x is ~0.3 (for ~24 800 wppm (~2.5 wt%)) in this study. The potential charge compensating mechanisms through vacancies or interstitials in the ianthinite are not discussed because they are beyond the scope of this study.

3.2.2. Becquerelite

The starting leachant compositions for Ce and Nd tests were 2.1 wppm and 277 wppm, respectively. EELS analysis was performed on becquerelite particles that were sufficiently thin for microanalysis. The cerium concentration in becquerelite was below the limit of detection for the AEM/EELS technique. A uniform distribution of Nd was noted during the AEM/EELS examination of these samples (Fig. 6). The ICP–MS results (Table 2) from dissolved solids indicate that about 33 wppm Ce was present in the becquerelite, while neodymium content was much higher, being approximately 1310 wppm. The corresponding K_d values for Ce and Nd incorporations in this test were 17 and 5, respectively. This will be further discussed later in this section.

The structure of becquerelite consists of sheets of $Ur\phi_5$ pentagonal bipyramid polyhedra connected through hydrogen bonds to interlayer Ca^{2+} ions and water molecules [20,21]. The incorporation of Nd^{3+} into this structure is likely to occur by substituting for Ca^{2+} in the interlayer, assuming that appropriate charge compensating substitutions can occur ($^{[8]}Ca^{2+}$–O = 0.248 nm vs. $^{[8]}Nd^{3+}$–O = 0.247 nm [9]). The superscripts in square brackets indicate the number of total anions that bond to the cations. One possible substitution mechanism involves $O^{2-} \leftrightarrow OH^-$ in the structure. Therefore,

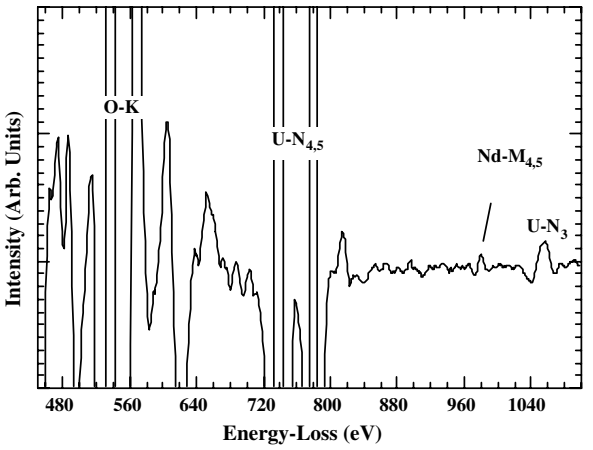

Fig. 6. Electron energy-loss spectrum of Nd-bearing becquerelite. The vertical scale intensity has been increased 50× for easier viewing of the Nd peak located at 980 eV.

Table 2
K_d values for Ce and Nd in becquerelite

	Leachant (wppm)	Leachate (wppm)	Becquerelite (wppm)[b]	K_d
Ce	2.1	2.1 (1.9[a])	33	17
Nd	277	271	1310	5

[a] Number calculated from weight of solid becquerelite and concentration of Ce in solid phase.
[b] Determined from ICP/MS analysis of the dissolved solids.

the suggested charge-coupled substitution will be $Nd^{3+} + O^{2-} \leftrightarrow Ca^{2+} + OH^-$. This is a reverse of the charge compensating mechanism proposed to occur during the substitution of Nd^{3+} in the structure of ianthinite. The balanced reaction for the substitution of Nd^{3+} for Ca^{2+} in the interlayer sites of becquerelite is proposed:

$$\begin{aligned} &Ca(UO_2)_6O_4(OH)_6(H_2O)_8 + xNd^{3+} \\ &\quad \Longleftrightarrow Ca_{1-x}Nd_x(UO_2)_6O_{4+x}(OH)_{6-x}(H_2O)_8 \\ &\qquad + xCa^{2+} + xH^+. \end{aligned} \tag{10}$$

The incorporation of Ce^{4+} into this structure is likely to occur by substitution for UO_2^{2+} within the $Ur\phi_5$ polyhedral sheet, together with local charge compensating substitutions ($Ce^{4+} + 2O^{2-} \leftrightarrow UO_2^{2+} + 2OH^-$). The Ce^{4+} ion could also possibly be accommodated in the interlayer sites of becquerelite by substituting for Ca^{2+} ($^{[8]}Ca^{2+}$–O = 0.248 nm vs. $^{[8]}Ce^{4+}$–O = 0.233 nm [9]).

A lower K_d value was obtained for Nd relative to Ce (see Table 2), suggesting that incorporation (ionic substitution and/or adsorption) of cerium is favored over that of neodymium in becquerelite. This may be due to the dependence of the K_d values on solution concentration (2.1 wppm Ce vs. 271 wppm Nd in leachate) as was also observed in the tests with ianthinite. A test with Nd concentration approximating that of Ce (2.1 wppm) was not conducted, and thus preference between the incorporation of cerium and neodymium in becquerelite from solutions with similar ionic strengths could not be determined.

3.2.3. Uranyl hydroxide compounds

Both SEM and EELS analyses were conducted on uranyl particles, the latter on crystals that were sufficiently thin for microanalysis. These analyses confirmed that the phase is of a uranium–oxide composition, however, neither technique was sensitive enough to detect any cerium in the solid. A heterogeneous distribution of neodymium was noted in crystals formed in tests where neodymium was added, suggesting that a separate neodymium-rich phase might have precipitated along with the uranyl hydroxide compound (Fig. 7). The formation of a separate neodymium-enriched phase may occur as a result of the relatively high concentration of neodymium in the leachant (Table 3) and/or the larger difference in valence charge between Nd^{3+} and U^{6+}, relative to Ce^{4+} and U^{6+}.

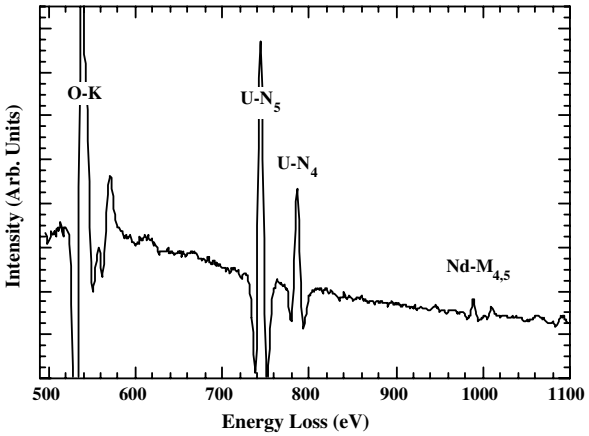

Fig. 7. Electron energy-loss spectrum of Nd-bearing regions in uranyl compounds. Further analysis indicated that the Nd was distributed in a heterogeneous manner, as other uranium-bearing regions did not contain detectable Nd.

Table 3
Concentration values (in wppm) and K_d values for Ce and Nd in uranyl compounds

	Test interval (days)	Leachant (wppm)	Leachate (wppm)	Uranyl solid (wppm)[a]	K_d	Leachate uranium (wppm)
Ce^{4+}	7	2.1	1.9	26	14	4238
Ce^{4+}	35	2.1	1.9	20	11	3315
Ce^{4+}	190	4.6	4.2	11	3	Not determined
Nd^{3+}	7	286	273	1240	5	3593
Nd^{3+}	35	286	270	922	3	3482

[a] Determined from ICP/MS analysis of the dissolved solids.

ICP–MS analyses indicate that the cerium concentration in the solid decreased from 26, to 20, and finally 11 wppm for crystals produced in 7-, 35-, and 190-day tests, respectively (Table 3). Uranium concentrations in the leachate solution also decreased from approximately 4200 to 3300 wppm between 7 and 35 days of testing. Due to analytical problems, uranium concentrations were not able to be obtained from the 190-day test. The decreases in cerium concentration occurred concurrently while the crystals became progressively coarser grained with increasing reaction time (Fig. 8). The relatively small increase in grain size between 7 and 35 days (compare Fig. 8(a) and (b)) resulted in a proportionally small decrease in cerium concentration (26–20 wppm). Between 35 and 190 days the crystals displayed a relatively large increase in grain size (compare Fig. 8(b) and (c)) and a correspondingly

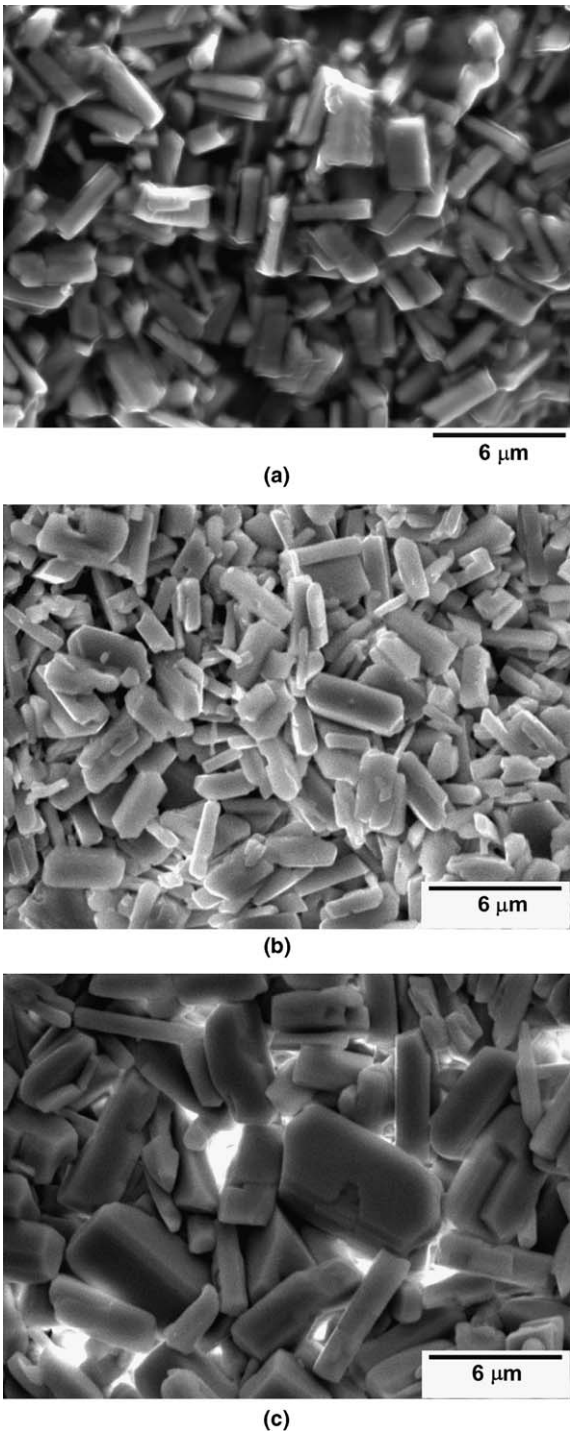

Fig. 8. SEM micrographs of the uranyl hydroxide phase: (a) 7-day sample, (b) 35-day sample, and (c) 190-day samples. Note that crystals become increasingly coarser grained with increasing reaction time.

larger decrease in cerium concentration (20–11 wppm). The pattern of decreasing cerium content can thus be correlated with grain size, with the 190-day test displaying the formation of the largest crystals and lowest cerium concentrations.

The inverse correlation observed between crystal grain size and cerium content suggests a mechanism whereby the cerium content in solution is being controlled by surficial processes on the solid. There are two potential mechanisms by which surficial adsorption may be influenced by growth of crystals in these tests. The first mechanism involves preferential adsorption of Ce-containing aqueous complexes at the higher-energy defect sites located at edges and/or corners of the uranyl hydroxide crystals. The relatively smaller sized crystals would have a proportionally higher number of such defect sites relative to sites located along flat surfaces and fully coordinated sites located in the center of the crystals. Formation of larger crystals would reduce the availability of high-energy surface defects sites relative to the flat crystal surface and interior sites through a decreasing of the surface area/volume ratio of the crystals. Such a process could be responsible for the observed decrease in REE sorption on the crystals. A second potential mechanism that may affect the uptake of cerium by the crystals may be related to the rate of crystal precipitation. The content of cerium in the crystals was highest where uranium content was also the highest in solution. During stages of rapid growth kinetics, the crystal surfaces may be less selective for foreign atoms, thereby allowing a greater proportion of Ce^{4+} atoms to become adsorbed to the crystals. Continued rapid crystal growth in such an environment may eventually trap adsorbed cerium atoms by surficial overgrowth processes. Growth kinetics of the crystals would be expected to slow as uranium solution concentrations decreased in the longer-term tests. The crystals may become more selective against foreign specie atoms like Ce^{4+} under such conditions, thereby limiting the amount of adsorbed cerium to the surface and/or desorbing cerium that had been previously attached.

Surface adsorption processes may dominate cerium retention by the uranyl hydroxide phase produced in the present set of tests and for other uranyl compounds as well. Adsorption processes for the uranyl hydroxide solid was further characterized by calculating K_d values for cerium adsorption. The calculated K_d values were 14, 11, and 3 for the 7-, 35-, and 190-day tests, respectively (Table 3). The K_d value of 3 for the 190-day test represents our best current estimate for long-term adsorption

Table 4
Summary of Ce (surrogate for Pu) and Nd (surrogate for Am) tests in uranium alteration phases

Uranium alteration phases	Test interval (days)	Ce in leachant (wppm)	Ce in leachate (wppm)	Ce in solid (wppm)[a]	K_d	Nd in leachant (wppm)	Nd in leachate (wppm)	Nd in solid (wppm)[a]	K_d
Ianthinite[b]	7	2.1	0.3	306	1020	399	216	24800	115
	7	–	–	–	–	9.8	0.7	588	840
Becquerelite	7	2.1	2.1 (1.9[c])	33	17	277	271	1310	5
Uranyl hydroxide	7	2.1	1.9	26	14	286	273	1240	5
compound	35	2.1	1.9	20	11	286	270	922	3
	190	4.6	4.2	11	3	–	–	–	–

[a] Determined from ICP/MS analysis of the dissolved solids.
[b] In ianthinite tests, Ce^{4+} might have been reduced to Ce^{3+}.
[c] Number calculated from weight of solid becquerelite and concentration of Ce in solid phase.

potential by uranyl hydroxide crystals. However, dehydrated schoepite crystals observed following decade-long corrosion studies with UO_2 have crystalline dimensions that are typically an order of magnitude larger than the uranyl hydroxide phase observed in the present set of tests [2,3]. Thus, the K_d values for Ce^{4+} incorporation in a uranyl hydroxide phase may be even lowered further (<3) for larger crystals produced during the long-term corrosion of spent fuel.

The neodymium distributions follow a parallel trend as was observed in the cerium tests. The ICP–MS results (Table 3) from the dissolved uranyl solids indicate an overall composition of 1240 wppm neodymium in the 7-day test, and 922 wppm after 35 days. The starting leachant composition for neodymium was 286 wppm. The corresponding K_d values were 5 and 3, respectively. It is difficult to interpret these results directly with respect to a single crystalline phase, however, since the microscopic examinations of crystals from tests with the neodymium solution indicate the presence of more than one crystalline phase (as previously discussed).

4. Conclusions

The potential for REE incorporation into or onto uranium alteration phases has been evaluated by precipitating uranyl phases from aqueous solutions containing cerium or neodymium. The REEs serve as both monitors for evaluating the potential repository behavior of tri- and quadravalent REE radionuclides and as surrogates for actinides (e.g., Ce^{4+} and Nd^{3+} for Pu^{4+} and Am^{3+}, respectively). The determined K_d values for REE incorporation remained greater than one for all cerium and neodymium tests conducted (Table 4), indicating a preference of the REE for incorporation into/onto the uranyl phases. The highest K_d values obtained for both cerium and neodymium were for ianthinite, which was consistent with earlier predictions based upon the crystal structure of ianthinite containing both U^{4+} and U^{6+} [12]. Solution concentrations of the lanthanide elements appeared to be inversely correlated with the K_d values, with higher K_d values occurring at lower concentrations. A similar behavior was noted between the incorporation of cerium and neodymium in ianthinite at similar ionic strengths suggesting that Ce^{4+} might have been reduced to Ce^{3+} in test solutions, thus explaining its similar behavior to Nd^{3+}. Incorporation of cerium and neodymium into becquerelite is predicted to be accomplished by co-precipitation of these elements within the crystalline structure, substituting for UO_2^{2+} or for interlayer cation Ca^{2+}. A decrease in the REE concentrations in the uranyl hydroxide compounds with increasing reaction time could be correlated with both a coarsening of the crystals and a decrease in uranium concentration in the leachate solution. These correlations suggest a lowering of the potential for REE incorporation as the overall surface area/volume ratio of the crystals and/or the kinetic rate of crystal formation decreases. Adsorption onto the surfaces of uranyl phases may thus play a key role in the immobilization of REE, and by analogy, the behavior of tri- and quadravalent actinides may similarly be affected. This role will be enhanced when particular crystalline phases are relatively abundant and/or the activity of a specific radionuclide is relatively low. Therefore, the migration of radionuclides during spent nuclear fuel corrosion in an oxidizing environment can be predicted to be constrained by possible retention (adsorption and/or ionic substitu-

tion) of the radionuclides into the alteration phases of spent nuclear fuel under such conditions.

Acknowledgement

This work was supported by the US Department of Energy, Environmental Management Science Program, under contract DE-FG07-97ER14820. The AEM investigations were performed at Argonne National Laboratory. Discussions with William Murphy were particularly enlightening with respect to potential precipitation kinetic effects on trace element partitioning.

References

[1] J.O. Barner, Pacific Northwest Laboratory Report PNL–5109 (1985).
[2] D.J. Wronkiewicz, J.K. Bates, S.F. Wolf, E.C. Buck, J. Nucl. Mater. 238 (1996) 78.
[3] D.J. Wronkiewicz, J.K. Bates, T.J. Gerding, E. Veleckis, B.S. Tani, J. Nucl. Mater. 190 (1992) 107.
[4] P.A. Finn, J.C. Hoh, S.F. Wolf, S.A. Slater, J.K. Bates, Radiochim. Acta 74 (1996) 65.
[5] W.M. Murphy, E.C. Pearcy, Mater. Res. Soc. Symp. Proc. 257 (1992) 521.
[6] P.C. Burns, R.C. Ewing, M.L. Miller, J. Nucl. Mater. 245 (1997) 1.
[7] E.C. Buck, R.J. Finch, P.A. Finn, J.K. Bates, Mater. Res. Soc. Symp. Proc. 506 (1998) 87.
[8] E.C. Buck, D.J. Wronkiewicz, P.A. Finn, J.K. Bates, J. Nucl. Mater. 249 (1997) 70.
[9] R.D. Shannon, Acta Cryst. A32 (1976) 751.
[10] R.J. Finch, R.C. Ewing, Mater. Res. Soc. Symp. Proc. 333 (1994) 625.
[11] E.C. Pearcy, J.D. Prikryl, W.M. Murphy, B.W. Leslie, Appl. Geochem. 9 (1994) 713.
[12] P.C. Burns, R.J. Finch, F.C. Hawthorne, M.L. Miller, R.C. Ewing, J. Nucl. Mater. 249 (1997) 199.
[13] R.J. Finch, E.C. Buck, P.A. Finn, J.K. Bates, Mater. Res. Soc. Symp. Proc. 556 (1999) 431.
[14] C. Bignand, Bull. Soc. Franç. Minér. Crist. 78 (1955) 1.
[15] E.H.P. Cordfunke, G. Prins, P.V. Vlaanderen, J. Inorg. Nucl. Chem. 30 (1968) 1745.
[16] R.J. Finch, F.C. Hawthorne, R.C. Ewing, Can. Miner. 36 (1998) 831.
[17] J.C. Taylor, Acta Crystallogr. B27 (1971) 1088.
[18] Handbook of Chemistry and Physics, 67th ed., CRC Press, Inc., 1986–1987.
[19] D. Langmuir, Aqueous Environmental Geochemistry, Prentice-Hall, Inc., 1997.
[20] P.C. Burns, M.L. Miller, R.C. Ewing, Can. Miner. 34 (1996) 845.
[21] M.K. Pagoaga, D.E. Appleman, J.M. Stewart, Am. Mineral. 72 (1987) 1230.